AIP | Physics of Plasmas

Chaotic coordinates for the Large Helical Device

S. R. Hudson and Y. Suzuki

Citation: Physics of Plasmas (1994-present) **21**, 102505 (2014); doi: 10.1063/1.4897390
View online: http://dx.doi.org/10.1063/1.4897390
View Table of Contents: http://scitation.aip.org/content/aip/journal/pop/21/10?ver=pdfcov
Published by the AIP Publishing

Chaotic coordinates for the Large Helical Device

S. R. Hudson[1,a)] and Y. Suzuki[2]
[1]Princeton Plasma Physics Laboratory, P.O. Box 451, Princeton, New Jersey 08543, USA
[2]National Institute for Natural Sciences, National Institute for Fusion Sciences, 322-6 Oroshi, Toki, 509-5292, Japan

(Received 9 July 2014; accepted 24 September 2014; published online 14 October 2014)

The theory of quadratic-flux-minimizing (QFM) surfaces is reviewed, and numerical techniques that allow high-order QFM surfaces to be efficiently constructed for experimentally relevant, non-integrable magnetic fields are described. As a practical example, the chaotic edge of the magnetic field in the Large Helical Device (LHD) is examined. A precise technique for finding the boundary surface is implemented, the hierarchy of partial barriers associated with the near-critical cantori is constructed, and a coordinate system, which we call chaotic coordinates, that is based on a selection of QFM surfaces is constructed that simplifies the description of the magnetic field, so that flux surfaces become "straight" and islands become "square." © *2014 AIP Publishing LLC*.
[http://dx.doi.org/10.1063/1.4897390]

I. INTRODUCTION

The study of dynamical systems is greatly facilitated by a coordinate framework with coordinate surfaces that coincide with structures that are invariants of the dynamical flow. Integrable Hamiltonian systems, by definition, possess a continuous family of invariant *action* surfaces, and action-angle coordinates may be constructed.[1] In these coordinates, the dynamics becomes trivial.

Non-integrable Hamiltonian systems, by definition, do not. Nevertheless, action-angle-*like* coordinates can still be constructed that simplify the description of the dynamics where it is possible to do so. After an integrable system is generally perturbed, the Poincaré-Birkhoff theorem,[2–4] the Aubry-Mather theorem,[5,6] and the KAM theorem,[2–4] named after Kolmogorov,[7] Arnold,[8] and Moser,[9] show that there are important, "regular" structures that remain invariant under the perturbed dynamics. Coordinates adapted to a selection of these invariant sets, which we call chaotic coordinates, provide substantial advantages: the regular motion becomes straight, by which it is meant that the generalized position coordinate increases linearly against the time coordinate under the dynamical flow and the generalized momentum coordinate is constant. The irregular motion is bounded by, and dissected by, coordinate surfaces that coincide with surfaces of locally minimal flux.

The magnetic fields used in tokamaks, such as the ITER[10] experiment currently under construction in France, and stellarators and heliotrons, such as the W7X[11] experiment being built in Germany, are analogous to $1\frac{1}{2}$-dimensional Hamiltonian systems; so the above-mentioned theorems of Hamiltonian mechanics are directly relevant to the study of magnetically confined plasmas. In the magnetic-confinement community, action-angle coordinates are called "straight-fieldline" coordinates.

To illustrate the construction of chaotic coordinates for an experimentally relevant magnetic field, this paper will study the magnetic field in the Large Helical Device (LHD), a device of the heliotron class in operation in Japan.[12]

Idealized tokamaks are axisymmetric and thus, by Noether's theorem,[1] have integrable magnetic fields. Stellarators and heliotrons are designed so that the magnetic fields are as close-to-integrable as is possible, and methods for eliminating the magnetic islands that destroy integrability have been developed;[13,14] however, small imperfections, plasma instabilities, and/or intentionally applied error fields[15] in the tokamak class, and the inherently three-dimensional nature of stellarators and heliotrons, destroy integrability.

To generalize the construction of straight-fieldline coordinates to arbitrarily perturbed magnetic fields, we generalize the construction of invariant action surfaces to *almost*-invariant, quadratic-flux-minimizing (QFM) surfaces introduced by Dewar *et al.*[16] The construction of QFM surfaces enabled the "island-healing" technique[17] used in the design of the National Compact Stellarator Experiment.[18]

In Sec. II, we recall the formalism of Lagrangian variational calculus for constructing magnetic fieldlines as extrema of the action integral. The extension of this theory leading to the definition of the quadratic-flux functional, the derivation of the Euler-Lagrange equations for extremal surfaces, and the introduction of the *pseudo* magnetic field is given in Sec. II A, in what is, hopefully, a more concise and transparent fashion than that given previously.[19]

In earlier work,[14,17] periodic QFM surfaces were constructed by finding families of periodic fieldlines of the pseudo field by fieldline integration. In Sec. III A, we introduce the pseudo *tangent* map that makes this algorithm more efficient. An alternative numerical construction is introduced in Sec. III B that allows high-order pseudo fieldlines to be constructed by finding *constrained* extrema of the action integral.

A definition of "chaotic coordinates" is given in Sec. IV. These coordinates are adapted to the invariant structures of non-integrable fields, namely, the periodic orbits and the irrational KAM surfaces and cantori, which can be closely

a)Electronic mail: shudson@pppl.gov

approximated by periodic orbits, and are based on a selection of rational QFM surfaces. A practical definition of the poloidal angle is introduced, so that the pseudo fieldlines become straight. A hierarchy of chaotic coordinates can be constructed: the consequences of choosing different rational QFM surfaces that serve as the coordinate framework are discussed in Sec. IV A. How the construction of QFM surfaces allows an approximation to the island separatrices to be determined is described in Sec. IV B, and Mather's difference-in-action[20] is reviewed in Sec. IV C.

In Sec. V, we describe the discretization of the action integral with an arbitrary vector potential (with a convenient choice of gauge, the Appendix) using a piecewise-linear, piecewise-constant representation of an arbitrary, *trial* curve. This provides a particularly efficient numerical method as (i) the required integrals can be calculated analytically, so that the action integral becomes an analytic function of the independent degrees-of-freedom that represent the trial curve; and (ii) the Hessian matrix of second partial derivatives is tridiagonal, Sec. V A, and thus is simple to invert. The calculation of Greene's residue[21] using the action formalism[22] is generalized for an arbitrary magnetic field, Sec. V B.

We present some example calculations for LHD in Sec. VI. First, we construct an example of "low-resolution" chaotic coordinates, Sec. VI A, and use these coordinates to construct a selection of high-order periodic orbits that approximate irrational KAM surfaces and cantori. An algorithm based on Greene's residue criterion is employed to identify the last closed magnetic surface, which following Greene *et al.*[23] we hereafter call the boundary surface. Realizing that the cantori will form effective barriers to transport in non-ideal plasmas, as discussed in Sec. VI B, the strength of a hierarchy of partial barriers is quantified by computing the flux Farey tree. Finally, in Sec. VI C, "high-resolution" chaotic coordinates are illustrated, for which more of the geometrical complexity of the magnetic fieldline flow is incorporated directly into the coordinates, so that the flux surfaces become "straight" and the islands become "square."

II. INVARIANT CURVES AND ALMOST-INVARIANT SURFACES

For a given magnetic field, $\mathbf{B} \equiv \nabla \times \mathbf{A}$, where $\mathbf{A}$ is a suitable vector potential, the magnetic-fieldline action, $S[\mathcal{C}]$, is the line integral[24]

$$S[\mathcal{C}] \equiv \oint_{\mathcal{C}} \mathbf{A} \cdot d\mathbf{l}\,, \tag{1}$$

where $d\mathbf{l}$ is an infinitesimal line segment parallel to an arbitrary *trial curve*, $\mathcal{C}$. In toroidal coordinates, (ρ, θ, ζ), a trial curve may be described by $\theta \equiv \theta(\zeta)$ and $\rho \equiv \rho(\zeta)$; where ρ is a radial label, θ is a poloidal angle, and the toroidal angle, ζ, is used to parametrize position along the curve. The coordinates may be defined via the inverse transformation, e.g., $R \equiv R(\rho, \theta, \zeta)$, $\phi \equiv \zeta$ and $Z \equiv Z(\rho, \theta, \zeta)$, where position is $\mathbf{x} \equiv R\cos\phi\,\mathbf{i} + R\sin\phi\,\mathbf{j} + Z\,\mathbf{k}$.

Magnetic fieldlines are those particular curves for which the action is stationary. The first-order variation in S allowing for arbitrary variations $\delta\rho(\zeta)$ and $\delta\theta(\zeta)$ is

$$\delta S = \int_{\mathcal{C}} d\zeta \left(\delta\theta \frac{\delta S}{\delta\theta} + \delta\rho \frac{\delta S}{\delta\rho} \right), \tag{2}$$

where the Frechét derivatives are

$$\frac{\delta S}{\delta\theta} \equiv \sqrt{g} B^{\rho} - \dot{\rho}\sqrt{g} B^{\zeta}, \tag{3}$$

$$\frac{\delta S}{\delta\rho} \equiv \dot{\theta}\sqrt{g} B^{\zeta} - \sqrt{g} B^{\theta}, \tag{4}$$

and the "dot" denotes the total derivative with respect to ζ. The equations describing a fieldline are obtained by setting each of the Frechét derivatives to zero.

To define a unique fieldline, it is necessary to provide suitable constraints. The standard approach[1] is to specify the endpoints of a finite-length curve. Another possibility is to enforce periodicity: periodic curves are, in a practical sense, of finite length. Trial curves are (p, q)-periodic if $\theta(\zeta + 2\pi q) = \theta(\zeta) + 2\pi p$ and $\rho(\zeta + 2\pi q) = \rho(\zeta)$, where p and q are relatively prime integers. A family of angle-curves is described by $\theta_\alpha(\zeta) \equiv \alpha + p\,\zeta/q + \tilde{\theta}_\alpha(\zeta)$, where $\tilde{\theta}_\alpha(0) = \tilde{\theta}_\alpha(2\pi q) = 0$, and α will be used as a fieldline label.

A. Extremizing surfaces and the pseudo field

The construction of extremal *curves* of the *action* integral can be generalized to the construction of extremal *surfaces* of the *quadratic-flux* integral. Consider a single-valued, *trial surface* $\rho \equiv P(\theta, \zeta)$. Together with a family of periodic angle-curves, this defines a family of periodic radial-curves via $\rho_\alpha(\zeta) \equiv P(\theta_\alpha(\zeta), \zeta)$, which in turn locally defines the *pseudo* radial dynamics

$$\dot{\rho} \equiv \partial_\theta P \dot{\theta} + \partial_\zeta P. \tag{5}$$

The tangent vector to any set of curves in space locally defines a vector field; so the pseudo dynamics defines a *pseudo*-field, $\mathbf{B}_\nu \equiv \dot{\rho}\, B^\zeta\, \mathbf{e}_\rho + \dot{\theta}\, B^\zeta \mathbf{e}_\theta + B^\zeta\, \mathbf{e}_\zeta$, on the trial surface that has the $\theta_\alpha(\zeta)$ and $\rho_\alpha(\zeta)$ as integral curves.

There is sufficient freedom to generally assume that each $\theta \equiv \theta_\alpha(\zeta)$ satisfies the true angle-dynamics, i.e., we may choose angle-curves that satisfy

$$\dot{\theta} \equiv \frac{\sqrt{g} B^\theta}{\sqrt{g} B^\zeta}. \tag{6}$$

This is equivalent to enforcing the constraint $\delta S/\delta\rho = 0$.

We cannot generally *also* force the constraint that $\delta S/\delta\theta = 0$ along *each* trial curve on the trial surface. This would be tantamount to insisting that each trial curve is a periodic fieldline; but, from the theory of perturbed Hamiltonian dynamical systems,[4] it is well known that rational invariant surfaces do not generally exist and the *action-gradient*, $\nu \equiv \delta S/\delta\theta$, is generally non-zero.

Using the true angle-dynamics and allowing for arbitrary radial dynamics, so that Eq. (3) becomes $\dot{\rho}\, B^\zeta = B^\rho - \nu/\sqrt{g}$, the pseudo-field defined by Eq. (5) is

$$\mathbf{B}_\nu = \mathbf{B} - \mathbf{e}_\rho\, \nu/\sqrt{g}, \tag{7}$$

where the action-gradient implied by a given trial surface is $\nu/\sqrt{g} = B^\rho - \partial_\theta P B^\theta - \partial_\zeta B^\zeta$.

Even though it is not generally possible to construct trial surfaces so that $\delta S/\delta\theta = 0$ along each trial curve, we can construct surfaces that minimize the *quadratic-flux* functional[16] defined as

$$\varphi_2 = \frac{1}{2}\int\int d\theta d\zeta \left(\frac{\delta S}{\delta\theta}\right)^2. \tag{8}$$

Allowing the trial surface to vary, $\delta P(\theta,\zeta)$, the first order variation in φ_2 is

$$\delta\varphi_2 = \int\int d\theta d\zeta \nu[\delta(\sqrt{g}B^\rho) - \delta\dot{\rho}\,\sqrt{g}B^\zeta - \dot{\rho}\,\delta(\sqrt{g}B^\zeta)].$$

From Eq. (5) and using Eq. (6)

$$\delta\dot{\rho}\,\sqrt{g}B^\zeta = \partial_\theta\delta P\,\sqrt{g}B^\theta + \partial_\zeta\delta P\,\sqrt{g}B^\zeta + \partial_\theta P\,\partial_\rho(\sqrt{g}B^\theta)\,\delta P - \partial_\theta P\,\dot{\theta}\,\partial_\rho(\sqrt{g}B^\zeta)\,\delta P.$$

Integrating by parts

$$-\int\int d\theta d\zeta\,\nu\,\partial_\beta\delta P\,\sqrt{g}B^\beta = \int\int d\theta d\zeta \delta P\, d_\beta(\sqrt{g}B^\beta\nu),$$

and recognizing that the total derivative with respect to the angles $\beta = \theta,\zeta$ must accommodate the dependency $\rho \equiv P(\theta,\zeta)$, so that

$$d_\beta(\sqrt{g}B^\beta\nu) = \partial_\rho(\sqrt{g}B^\beta)\,\partial_\beta P\,\nu + \partial_\beta(\sqrt{g}B^\beta)\,\nu + \sqrt{g}B^\beta\,\partial_\beta\nu,$$

and using $\nabla\cdot\mathbf{B} = 0$, the first-order variation in φ_2 is

$$\delta\varphi_2 = \int\int d\theta d\zeta\,\delta P\,(\sqrt{g}B^\theta\partial_\theta + \sqrt{g}B^\zeta\partial_\zeta)\nu. \tag{9}$$

The Euler-Lagrange equation for extremizing surfaces is that the action-gradient is constant along the angle-dynamics, $(B^\theta\partial_\theta + B^\zeta\partial_\zeta)\nu = 0$. The angle-dynamics, together with $\rho \equiv P(\theta,\zeta)$, defines the pseudo-field, and so ν is constant along the fieldlines of $\mathbf{B}_\nu$.

We now describe two numerical algorithms for constructing QFM surfaces as families of periodic, pseudo-fieldlines; the first is based on fieldline integration, and the second is based on a constrained-area, action-minimizing, variational principle.

III. NUMERICAL CONSTRUCTION

The *true* fieldline flow induced by a given field, $\mathbf{B}$, produces a mapping, M^q, from an initial point, (θ_0,ρ_0), on the Poincaré section $\zeta = 0$ around q toroidal periods to arrive at (θ_q,ρ_q)

$$\begin{pmatrix}\theta_q\\ \rho_q\end{pmatrix} = M^q\begin{pmatrix}\theta_0\\ \rho_0\end{pmatrix}. \tag{10}$$

Periodic fieldlines are fixed points of M^q, with the understanding that $2\pi p$ is to be subtracted from θ_q.

In the integrable case, a continuous family of periodic fieldlines exists, each of which may be labeled by α and which may be found by a one-dimensional search in ρ for each given θ_0. In the general, non-integrable case, typically only two distinct periodic fieldlines exist for a given periodicity, the so-called Poincaré-Birkhoff periodic orbits,[2,22] which are located say at $\theta = \alpha_X$ and $\theta = \alpha_O$.

The behavior of fieldlines near a given fieldline is described by the tangent map

$$\begin{pmatrix}\delta\theta_q\\ \delta\rho_q\end{pmatrix} = \nabla M^q\cdot\begin{pmatrix}\delta\theta_0\\ \delta\rho_0\end{pmatrix}, \tag{11}$$

which may be determined by fieldline integration

$$\frac{d}{d\zeta}\nabla M^q = \begin{pmatrix}\partial_\theta\dot{\theta}, & \partial_\rho\dot{\theta}\\ \partial_\theta\dot{\rho}, & \partial_\rho\dot{\rho}\end{pmatrix}\cdot\nabla M^q, \tag{12}$$

from the initial condition $\nabla M^q =$ the 2×2 identity matrix. If the eigenvalues of ∇M^q are complex conjugates, the tangent fieldlines will display elliptical motion and that periodic fieldline is considered "stable." If the eigenvalues are real reciprocals, the tangent motion will either exponentially grow or decay and the periodic fieldline is "unstable."

It is convenient at this point to recall Greene's residue criterion:[21,25] the existence of an invariant surface with irrational rotational-transform, $\imath$, is related to the stability of periodic fieldlines that "best approximate" the given irrational. The rational *convergents*,[26] (p_i, q_i), of a given irrational, $\imath$, form a sequence such that $p_i/q_i \to \imath$ as $i\to\infty$, and $|p_i/q_i - \imath| < |p/q - \imath|$ for all $q < q_i$. Greene introduced a quantity called the residue

$$R(p,q) = (2 - \lambda - \lambda^{-1})/4, \tag{13}$$

where λ and λ^{-1} are the eigenvalues of ∇M^q. If the residues of the convergents approach zero, $R(p_i,q_i)\to 0$ as $i\to\infty$, then the irrational surface will exist. If, however, the magnitude of the residues become large, $|R(p_i,q_i)|\to\infty$, then the surface has been destroyed by island-overlap[27] and the ensuing chaos. The critical value is 0.25. If $R(p_i,q_i)\to 0.25$, then the irrational surface is on the "edge of destruction" and is continuous but no longer smooth.

A. Pseudo-fieldline integration

Numerically, constructing QFM surfaces is very similar to finding periodic fieldlines. A (p, q)-QFM surface is a family of (p, q)-periodic fieldlines of the pseudo-field, $\mathbf{B}_\nu$, along each of which the action-gradient is constant, i.e., $\nu = \nu(\alpha)$. The task of finding these periodic pseudo fieldlines is equivalent to finding fixed points of the q-th return *pseudo*-map, which is constructed by integrating along the pseudo-field from an initial point, (θ_0,ρ_0), on the Poincaré section, e.g., $\zeta = 0$, around q toroidal periods to arrive at (θ_q,ρ_q). Given that ν is constant along the pseudo-field but that the particular numerical value of ν is not yet known, it is required to find the particular pair (ν,ρ_0) that gives a periodic, integral curve of $\mathbf{B}_\nu$ at the prescribed angle, $\theta_0 = \alpha$. The q-th return pseudo-map, P^q, is defined by

$$\begin{pmatrix}\theta_q\\ \rho_q\end{pmatrix} = P^q\begin{pmatrix}\nu\\ \rho_0\end{pmatrix}, \tag{14}$$

where the dependence on θ_0 is suppressed.

The q-th return, pseudo tangent-map, ∇P^q, is defined by

$$\begin{pmatrix}\delta\theta_q\\ \delta\rho_q\end{pmatrix} = \nabla P^q\cdot\begin{pmatrix}\delta\nu\\ \delta\rho_0\end{pmatrix}, \tag{15}$$

and can also be determined by pseudo fieldline integration over $\zeta\in[0,2\pi q]$ by

$$\frac{d}{d\zeta}\nabla P^q = \begin{pmatrix}\partial_\theta\dot\theta & \partial_\rho\dot\theta\\ \partial_\theta\dot\rho & \partial_\rho\dot\rho\end{pmatrix}\cdot\nabla P^q + \begin{pmatrix}0 & 0\\ 1/\sqrt{g}B^\zeta & 0\end{pmatrix},$$

with the initial condition

$$\nabla P^q = \begin{pmatrix}0 & 0\\ 0 & 1\end{pmatrix}. \tag{16}$$

The pseudo tangent map allows an efficient Newton iterative algorithm for finding fixed points: a correction, $(\delta\nu,\delta\rho)$, to an initial guess for (ν,ρ) is determined by requiring the pseudo fieldline be periodic

$$\begin{pmatrix}\theta_q\\ \rho_q\end{pmatrix} + \nabla P^q\cdot\begin{pmatrix}\delta\nu\\ \delta\rho_0\end{pmatrix} = \begin{pmatrix}\theta_0+2\pi p\\ \rho_0+\delta\rho\end{pmatrix}. \tag{17}$$

For the integrable case, for which there is a true periodic orbit for every value of the poloidal angle, the iterative solution will yield $\nu(\alpha)=0$ for all α, and the pseudo field reduces to the true field; and similarly for the non-integrable case: where true periodic fieldlines exist, e.g., at α_X and α_0, the solution yields $\nu(\alpha_X)=0$ and $\nu(\alpha_O)=0$.

At all angle locations where a periodic *true* fieldline does not exist, a periodic *pseudo* fieldline can still be constructed by suitably choosing ν. Intuitively, we may think of $\nu/\sqrt{g}$ as the amount of radial field that must be subtracted from the true field to "cancel" the resonant effect of the perturbation, and by so doing create a rational "pseudo" surface as a family of rational pseudo fieldlines.

B. Constrained, extremal curves

Another construction of pseudo fieldlines is obtained by realizing that curves that extremize the action subject to a constraint on the "area"

$$a \equiv \int_{-\pi q}^{+\pi q}\theta(\zeta)\,d\zeta, \tag{18}$$

are also integral curves of $\mathbf{B}_\nu$ with constant ν. The constrained-area, action integral is

$$F \equiv \oint_{\mathcal{C}}\mathbf{A}\cdot d\mathbf{l} - \nu\left(\oint_{\mathcal{C}}\theta\,\nabla\zeta\cdot d\mathbf{l} - a\right), \tag{19}$$

where formally ν is a Lagrange multiplier and a is the required numerical value of the area. Recalling that the change in $\int\mathbf{v}\cdot d\mathbf{l}$ due to changes, $\delta\mathbf{l}$, in only the curve is given by $\int(\nabla\times\mathbf{v})\times\delta\mathbf{l}\cdot d\mathbf{l}$, the first order variation in F is

$$\delta F = \int_{\mathcal{C}} d\mathbf{l}\times(\mathbf{B}-\nu\,\nabla\theta\times\nabla\zeta)\cdot\delta\mathbf{l}\,, \tag{20}$$

from which we see that $\delta F=0$ for arbitrary $\delta\mathbf{l}$ along the integral curves of $\mathbf{B}_\nu\equiv\mathbf{B}-\nu\,\nabla\theta\times\nabla\zeta$. On using the coordinate identity $\nabla\theta\times\nabla\zeta=\mathbf{e}_\rho/\sqrt{g}$,[28] this is identical to the pseudo-field defined in Eq. (7).

Both the pseudo fieldline integration method, which seeks fixed points of the q-th return pseudo-map defined in Eq. (14), and the constrained-area, action-extremizing method, which seeks extrema of Eq. (19), will be used in the following to construct the periodic, pseudo fieldlines that comprise the QFM surfaces.

The pseudo fieldline integration method is simpler: all that is required is the magnetic field, $\mathbf{B}$, and suitable toroidal coordinates, (ρ,θ,ζ), so that $\mathbf{e}_\rho\equiv\sqrt{g}\,\nabla\theta\times\nabla\zeta$ may be defined.

The constrained-area, action-extremizing method is computationally faster and does not depend on integrating the ordinary differential equations that define the pseudo-field. This is a clear advantage for finding high-order (i.e., large q) periodic fieldlines and pseudo fieldlines in regions of chaos that would otherwise be swamped by the exponential increase of numerical error associated with finite Lyapunov exponents; however, this method requires an appropriate discretization of an arbitrary, periodic trial curve and the computation of the derivatives of the discretized action integral. How to construct these quantities will be described in Sec. V.

IV. CHAOTIC COORDINATES

The quadratic-flux functional depends on the action-gradient, which is *not* coordinate independent: the quantity $\delta S/\delta\theta$ depends on the choice of angle, θ, defined implicitly by the coordinate transformation and which, thus far, has been left as arbitrary. The arbitrariness in the choice of poloidal angle can be removed by the following convention: QFM surfaces are surfaces that minimize the quadratic-flux functional or equivalently comprised extremal curves of the constrained-area action functional, where the angle θ is such that the pseudo fieldlines are straight. Such an angle can be constructed iteratively.

Given a collection of N QFM surfaces, with different periodicities e.g., $(p_i,\ q_i)$ with $i=1,N$, that form a radial framework, and that have been constructed using an initial, arbitrary poloidal angle, it is possible to construct on each surface a new angle, $\bar\theta$, such that each pseudo curve is "straight," i.e., $\bar\theta=\alpha+p\,\zeta/q$. A Fourier decomposition of the cylindrical coordinates of each surface using the $(\bar\theta,\zeta)$ as angle coordinates, and a smooth interpolation of the Fourier harmonics between the surfaces, provides a global coordinate transformation, $R\equiv R(\psi,\bar\theta,\zeta)$ and $Z\equiv Z(\psi,\bar\theta,\zeta)$, where we have chosen to keep the usual, cylindrical toroidal angle, $\phi\equiv\zeta$, but this could be generalized to obtain a Boozer-like[29] toroidal angle, for example. It is convenient to label each pseudo-surface with the enclosed toroidal flux, $\psi\equiv(\text{toroidal flux})/2\pi$, and for the new fieldline-label, α,

we chose $\int(\alpha + p\,\zeta/q)\,d\zeta = \int\theta(\zeta)\,d\zeta$. We call the resulting coordinate framework *chaotic coordinates*. In chaotic coordinates, the Poincaré-Birkhoff orbits with the selected periodicities (p_i, q_i) are straight.

A. A hierarchy of chaotic coordinates

There is some freedom in the construction of chaotic coordinates, and a hierarchy of chaotic coordinates can be constructed that successively "straighten" more and more of the invariant, rational sets and thereby also the invariant, irrational sets. Practically, we must choose a finite selection of QFM surfaces that form the coordinate framework, and the selection will impact the resulting coordinates: the Poincaré-Birkhoff orbits with periodicities that correspond to the selected (p_i, q_i) are guaranteed to be straight, and those that do not are not.

The low-order rational QFM surfaces that pass through the low order islands will usually be quite smooth, and by selecting these surfaces as the coordinate framework we may construct coordinates that approximate straight-fieldline coordinates of some nearby, integrable field.

By taking suitable limits, the irrational, invariant sets guaranteed by the KAM theorem can be used as coordinate surfaces, and coordinate surfaces that "fill-in-the-gaps" in the cantori can be constructed.

As the size of the magnetic islands and the degree-of-chaos increases, the invariant sets become increasingly geometrically deformed, particularly the invariant sets that lie just outside the separatrices of large, low-order island chains. Theoretically, given that the rationals for a countable set, we may construct QFM surfaces for *all* rational periodicities present in the magnetic configuration; however, doing so would effectively be an attempt to construct straight fieldline coordinates globally, and the resulting hierarchy of chaotic coordinates will approach a non-smooth limit as the number of included QFM surfaces is increased if the magnetic field is chaotic.

These ideas will be described and illustrated in more detail in the following. Hereafter, the coordinates (ψ, θ, ζ) shall represent the chaotic coordinates for which the pseudo fieldlines for the selected periodicities are straight and lie on coordinate surfaces. To be formally precise, we should write $(\psi, \theta, \zeta)_{\mathbf{p},\mathbf{q}}$, where the subscript indicates the set of periodicities, (p_i, q_i), of the QFM surfaces that have been chosen as the coordinate framework; but this notation is clumsy, and in Sec. VI, where chaotic coordinates are shown for LHD, the selection of the (p_i, q_i) should be clear by context.

Before describing how the action integral may be discretized, we make some comments regarding the representation of the magnetic field, how to estimate the separatrix of an island chain, and how to compute the magnetic fieldline flux across a rational surface.

B. Island widths

Any magnetic field may be written

$$\mathbf{B} = \nabla\rho \times \nabla\theta - \nabla\chi(\rho,\theta,\zeta) \times \nabla\zeta, \tag{21}$$

where here the angle θ is arbitrary. The decomposition $\chi(\rho,\theta,\zeta) = \chi_0(\rho) + \tilde{\chi}_1(\rho,\theta,\zeta)$, where $\chi_0(\rho)$ is the average of $\chi(\rho,\theta,\zeta)$ on the surface $\rho \equiv$ const. for example, splits $\mathbf{B}$ into an integrable field plus a "perturbation" field. The (ρ,θ,ζ) coordinates and this decomposition are not unique, and the perturbation field may not be small.

Coordinates based on QFM surfaces offer certain advantages. The pseudo-field is formally only defined on the QFM surfaces; however, we may imagine that there is a globally defined integrable field, $\mathbf{B}_0 \equiv \nabla\psi \times \nabla\theta - \nabla\chi_0(\psi) \times \nabla\zeta$ that coincides with $\mathbf{B}_\nu$ where $\mathbf{B}_\nu$ is defined. Given that the periodic, pseudo fieldlines coincide with periodic, true fieldlines where the latter exist, from which it follows that the QFM surfaces reduce to rational flux surfaces where the latter exist; and that ν measures the difference between the true field and the pseudo-field, and that it is $\int\int d\theta d\zeta\,\nu^2/2$ that is minimized (formally, extremized) at the selected, *resonant* surfaces, which is where the effects of perturbations are the greatest; then, the $\mathbf{B}_0$ so defined is the "nearest" integrable field to the given magnetic field.

It is not the case that *all* the invariant surfaces of the true field, $\mathbf{B}$, will necessarily coincide with invariant surfaces of $\mathbf{B}_0$, just as it is not the case that the invariant, KAM surfaces of a perturbed field will coincide with the invariant surfaces of the unperturbed field. However, if in the construction of the (ψ,θ,ζ) coordinates a selection of rational pseudo surfaces with periodicities (p_i, q_i) that closely approximate a given irrational was chosen, then the pseudo surfaces will closely approximate that KAM surface, if it exists.

Specializing Eq. (21) to $\mathbf{B} = \nabla\psi \times \nabla\theta - \nabla\chi \times \nabla\zeta$, with $\psi = 0$ along the pseudo curves, then the expression for the action gradient given in Eq. (3) implies that $\nu = \sqrt{g}B^\psi = -\partial_\theta\tilde{\chi}_1$, and the size of the magnetic island that forms at the rational surface is determined by ν.

The generating function[4,30] $F(\bar{\psi},\theta,\zeta) \equiv (\theta - n\,\zeta/m)\,\bar{\psi}$ generates the canonical transformation to the rotating frame $\psi = \bar{\psi}$ and $\bar{\theta} = \theta - n\,\zeta/m$. The single-resonance Hamiltonian, $\chi(\psi,\theta,\zeta) \equiv \chi_0(\psi) + \chi_{n,m}\cos(m\theta - n\zeta)$, is transformed according to $\bar{\chi} \equiv \chi + \partial_\zeta F$ to give

$$\bar{\chi} = \chi_0(\psi) + \chi_{n,m}\cos(m\bar{\theta}) - n\,\psi/m.$$

Expanding about the rational surface, $\iota(\psi_{n/m}) \equiv \chi_0'(\psi_{n/m}) = n/m$, we obtain

$$\bar{\chi} = \frac{1}{2}\iota'\delta\psi^2 + \chi_{n,m}\cos(m\bar{\theta}), \tag{22}$$

where the constant terms, $\chi_0(\psi_{n/m})$ and $n\psi_{n/m}/m$ have been dropped. The island separatrix is defined by $\bar{\chi} = E = \chi_{n,m}$, which gives

$$\delta\psi = \pm\sqrt{2\chi_{n,m}[1 - \cos(m\bar{\theta})]/\iota'}. \tag{23}$$

C. Mather's difference-in-action

The magnetic flux through any surface is given by the integral $\int\mathbf{B}\cdot d\mathbf{s}$. If the surface is closed then the surface integral may be transformed into a volume integral $\int\nabla\cdot\mathbf{B}\,dv$, which is identically zero for divergence-free magnetic fields.

The surface integral can be converted to a line integral, $\oint\mathbf{A}\cdot d\mathbf{l}$, where $d\mathbf{l}$ is an infinitesimal line segment on the

boundary. The "upward" or "outward" flux across any surface passing through the islands, i.e., with boundary coinciding with the true periodic fieldlines, is given by the *difference-in-action*

$$\Delta W_{p/q} \equiv \int_O \mathbf{A}\cdot d\mathbf{l} - \int_X \mathbf{A}\cdot d\mathbf{l}, \tag{24}$$

introduced by Mather,[2,20] where the curve denoted by X represents the action-minimizing periodic fieldline, which is unstable, and that by O the action-minimax fieldline, which is usually stable for small perturbations from integrability. Computing the difference-in-action allows[20] another method for determining the existence of invariant, irrational KAM surfaces. If the limit $\Delta W_\iota \equiv \Delta W_{p_i/q_i}$ as $i \to \infty$ is zero, where (p_i, q_i) are the convergents of ι, then that irrational surface has no upward flux, i.e., the KAM surface exists. If $\Delta W_\iota \neq 0$, then ΔW_ι is the flux across the remnant cantorus, and ΔW_ι quantifies the importance of each cantorus as a partial barrier.

The construction of chaotic coordinates, along with a determination of Greene's residue, the estimate of the island separatrix, and computing Mather's difference-in-action, enables a sophisticated analysis of general magnetic fields. The following section, Sec. V, describes the discretization of the action integral and is largely technical. Readers primarily interested in the application to LHD can proceed to Sec. VI.

V. DISCRETIZED ACTION INTEGRAL

We now implement the action extremizing method. A discrete, piecewise-constant, piecewise-linear representation of a trial curve is employed.[31] For $\zeta \in [\zeta_{i-1}, \zeta_i]$

$$\begin{aligned}\rho(\zeta) &= \rho_i,\\ \theta(\zeta) &= \theta_{i-1} + \dot\theta(\zeta - \zeta_{i-1}),\end{aligned} \tag{25}$$

where $\dot\theta \equiv (\theta_i - \theta_{i-1})/\Delta\zeta$ is constant in (ζ_{i-1}, ζ_i), and $\Delta\zeta \equiv 2\pi/N$ where N is the number of line segments per 2π. Hereafter, to reduce notational clutter, we choose $N = 1$. The curve is constrained to be (p, q) periodic by setting $\theta_q \equiv \theta_0 + 2\pi p$. The $\{\rho_i : i = 1, q\}$ and the $\{\theta_i : i = 0, q-1\}$ are the $2q-1$ independent degrees-of-freedom that describe an arbitrary, periodic trial curve.

An arbitrary vector potential may be written

$$\mathbf{A} = A_\theta(\rho,\theta,\zeta)\nabla\theta + A_\zeta(\rho,\theta,\zeta)\nabla\zeta, \tag{26}$$

by a suitable choice of gauge (described in the Appendix). A Fourier representation will be used, so that for so-called stellarator-symmetric[32] fields we may write

$$\begin{aligned}A_\theta(\rho,\theta,\zeta) &= \sum\nolimits_j A_{\theta,j}(\rho)\cos(m_j\theta - n_j\zeta),\\ A_\zeta(\rho,\theta,\zeta) &= \sum\nolimits_j A_{\zeta,j}(\rho)\cos(m_j\theta - n_j\zeta).\end{aligned} \tag{27}$$

We restrict attention to stellarator-symmetric fields primarily for expedience; the following analysis is completely general, but stellarator-symmetric fields do provide some simplifications: the line $\theta = 0$, $\zeta = 0$ is a symmetry line, and the existence of symmetry lines makes finding the true periodic orbits particularly easy.

The action integral can be evaluated piecewise, $S \equiv \sum_i S_i$, where

$$S_i \equiv \int_{\zeta_{i-1}}^{\zeta_i} d\zeta\ \mathbf{A}\cdot\frac{d\mathbf{l}}{d\zeta} = \int_{\zeta_{i-1}}^{\zeta_i} d\zeta \sum\nolimits_j S_{i,j}, \tag{28}$$

where $S_{i,j} \equiv \mathcal{A}_{i,j}\cos(m_j\theta - n_j\zeta)$, and $\mathcal{A}_{i,j}(\rho,\theta_{i-1},\theta_i) \equiv A_{\theta,j}(\rho)\dot\theta + A_{\zeta,j}(\rho)$. An advantage of the piecewise-linear discretization for $\theta(\zeta)$ is that the integral of the trigonometric term can be evaluated analytically

$$\begin{aligned}C_{i,j}(\theta_{i-1},\theta_i) &\equiv \int_{\zeta_{i-1}}^{\zeta_i} d\zeta\cos(m_j\theta - n_j\zeta)\\ &= \frac{\sin\left(m_j\theta_i - n_j\zeta_i\right) - \sin\left(m_j\theta_{i-1} - n_j\zeta_{i-1}\right)}{m_j\dot\theta - n_j}.\end{aligned} \tag{29}$$

Care must be taken when $\delta \equiv m_j\dot\theta - n_j$ is small. Writing $\bar\alpha \equiv m_j\bar\theta - n_j\bar\zeta$, where $\bar\theta \equiv (\theta_{i-1} + \theta_i)/2$ and $\bar\zeta \equiv (\zeta_{i-1} + \zeta_i)/2$, the integral is well approximated by $C_{i,j}(\theta_{i-1},\theta_i) = \cos\bar\alpha\Delta\zeta[1 - \delta^2\Delta\zeta^2/24 + \mathcal{O}(\delta^4)]$. For brevity, we shall assume that Eq. (29) is valid.

A. Newton method

To find extremal curves, it is required to find extrema of $S \equiv \sum_{i,j} S_{i,j}(\rho_i,\theta_{i-1},\theta_i)$. The first derivatives are

$$\frac{\partial S_{i,j}}{\partial\rho_i} = \mathcal{A}_j' C_{i,j}, \tag{30}$$

$$\frac{\partial S_{i,j}}{\partial\theta_{i-1}} = -\frac{A_{\theta,j}(\rho_i)}{\Delta\zeta}C_{i,j} - \mathcal{A}_j(\rho_i)\frac{m\cos\alpha_{i-1,j}}{m_j\dot\theta - n_j} + \frac{S_{i,j}}{m_j\dot\theta - n_j}\frac{m}{\Delta\zeta}, \tag{31}$$

$$\frac{\partial S_{i,j}}{\partial\theta_i} = +\frac{A_{\theta,j}(\rho_i)}{\Delta\zeta}C_{i,j} + \mathcal{A}_j(\rho_i)\frac{m\cos\alpha_{i,j}}{m_j\dot\theta - n_j} - \frac{S_{i,j}}{m_j\dot\theta - n_j}\frac{m}{\Delta\zeta}, \tag{32}$$

where $\alpha_{i,j} \equiv m_j\theta_i - n_j\zeta_i$ and the prime denotes derivative with respect to ρ. A Newton method can be used to find extrema: given a suitable initial guess for the $\{\rho_i\}$ and the $\{\theta_i\}$, an iterative scheme that inverts the Hessian, i.e., the matrix of second partial derivatives, can be used.

Treating *all* of the $\{\rho_i\}$, the $\{\theta_i\}$, and the Lagrange multiplier, ν, as independent degrees-of-freedom requires inverting a matrix of size $\sim 2q \times 2q$, which requires $\mathcal{O}(2q)^3$ operations, and this becomes computationally infeasible for large q. Fortunately, the piecewise-constant piecewise-linear representation affords some further important simplifications.

The equation $\partial S/\partial\rho_i = 0$ reduces to $\partial S_i/\partial\rho_i = 0$. In each region, (ζ_{i-1}, ζ_i), ρ_i may be determined independently. Given θ_{i-1} and θ_i, we solve

$$\frac{\partial S_i(\rho_i,\theta_{i-1},\theta_i)}{\partial\rho_i} = 0, \tag{33}$$

for ρ_i. Generally this must be solved numerically, but a one-dimensional root finding algorithm that exploits the second

derivative information, $\partial^2 S_i/\partial\rho_i^2$, can rapidly solve this to machine precision. Inverting this equation for ρ, given $\dot{\theta}$, θ, and ζ, is always possible if the system has shear, $\dot{\theta}' \neq 0$. Hereafter, ρ_i is to be considered a function of θ_{i-1} and θ_i, i.e., $\rho_i = \rho_i(\theta_{i-1}, \theta_i)$, and the $\{\theta_i : i = 0, q-1\}$ alone completely describe the trial curve.

Extremal curves satisfy $\partial S/\partial\theta_i = 0$, where

$$\frac{\partial S}{\partial \theta_i} = \partial_2 S_i(\rho_i, \theta_{i-1}, \theta_i) + \partial_1 S_{i+1}(\rho_i, \theta_i, \theta_{i+1}), \tag{34}$$

and $\partial_1 S_i(\rho_i, \theta_{i-1}, \theta_i)$ and $\partial_2 S_i(\rho_i, \theta_{i-1}, \theta_i)$ are given by

$$\begin{aligned} \partial_1 S_i &= \frac{\partial S_i}{\partial \theta_{i-1}} + \frac{\partial S_i}{\partial \rho_i}\frac{\partial \rho_i}{\partial \theta_{i-1}}, \\ \partial_2 S_i &= \frac{\partial S_i}{\partial \theta_i} + \frac{\partial S_i}{\partial \rho_i}\frac{\partial \rho_i}{\partial \theta_i}, \end{aligned} \tag{35}$$

where

$$\frac{\partial \rho_i}{\partial \theta} = -\left(\frac{\partial^2 S_i}{\partial \theta \partial \rho_i}\right)\left(\frac{\partial^2 S_i}{\partial \rho_i^2}\right)^{-1}. \tag{36}$$

The equation of motion, $\partial_2 S_i + \partial_2 S_{i+1} = 0$ given in Eq. (34), has a form that may be familiar: if we use a model action with a "kinetic" term and a periodic potential, $S_i \equiv \frac{1}{2}(\theta_i - \theta_{i-1})^2 + k\cos\theta_i$ and employ the "velocity," $r_i \equiv \theta_i - \theta_{i-1}$, as the radial variable, then $\partial_2 S_i + \partial_2 S_{i+1} = 0$ becomes $r_{i+1} = r_i - k\sin\theta_i$ and $\theta_{i+1} = \theta_i + r_{i+1}$, which is widely used standard-map.[2]

Eliminating the ρ_i as degrees-of-freedom results in the action integral depending only on the θ_i, and the piecewise linear discretization results in the Hessian being cyclic-tridiagonal, which can be inverted in $\mathcal{O}(q)$ operations. If an additional constraint can be imposed, e.g., choosing $\theta_0 = 0$ to find the periodic fieldlines that lie on the symmetry line, then an additional degree-of-freedom can be removed and the Hessian becomes tridiagonal.

We have implemented a Newton method to solve the equations $\partial S/\partial\theta_i = 0$, for which it is required to compute the second-derivatives of the action integral. The total derivative of a function $S(\theta, \rho)$ with respect to θ, where ρ satisfies $F(\theta, \rho) = 0$, with respect to θ is given by the chain rule, $d_\theta S \equiv S_\theta + d_\theta \rho S_\rho$, where $d_\theta S$ denotes the total derivative of S, and S_θ denotes the partial derivative of S with respect to θ with ρ held constant, and vice-versa for S_ρ. The derivative of ρ with respect to θ is determined by requiring that $F(\theta, \rho) = 0$ remains satisfied as θ changes, $F_\theta d\theta + F_\rho d\rho = 0$. The second derivative of S is $d^2_{\theta\theta} S = (S_{\theta\theta} + d_\theta \rho S_{\theta\rho}) + d^2_{\theta\theta}\rho S_\rho + d_\theta \rho (S_{\rho\theta} + d_\theta \rho S_{\rho\rho})$, where the second derivative of ρ is

$$\frac{d^2\rho}{d\theta^2} = \frac{-(F_{\theta\theta} + d_\theta \rho F_{\theta\rho}) - d_\theta \rho (F_{\rho\theta} + d_\theta \rho F_{\rho\rho})}{F_\rho}.$$

The equation defining periodic pseudo fieldlines is simply $\partial S/\partial\theta_i = \nu$, where ν is a constant, i.e., ν does not depend on i. If ν is known, then a Newton algorithm that treats the θ_i as the only degrees-of-freedom is sufficient. This method was used (using a restricted choice of vector potential, so that $\rho = \dot{\theta}$ and inverting Eq. (33) became trivial) to locate the high-order, true periodic fieldlines (for which $\nu = 0$) that approximate cantori.[31] However, for locating pseudo fieldlines, ν is generally not known apriori.

To be consistent with the constrained-area, action-extremizing analysis, ν is a Lagrange multiplier and should be treated as an independent degree-of-freedom. This complicates the numerics because the Hessian loses the tridiagonal structure. It is instead preferable to split the iterative method so that it is similar to the algorithm described in Sec. III A. First, $\theta_0 \equiv \alpha$ is assumed to be given. Second, a guess for ν is provided. Third, a Newton correction, $\{\delta\theta_i : i = 1, q-1\}$, to the remaining degrees-of-freedom in trial curve is constructed by solving $\nabla\mathbf{D}(\boldsymbol{\theta}) \cdot \delta\boldsymbol{\theta} = -\mathbf{D}(\boldsymbol{\theta})$, where $\nabla\mathbf{D}_{i,j} \equiv \partial^2 F/\partial\theta_i\partial\theta_j$ is the Hessian and $\mathbf{D}_i \equiv \partial S/\partial\theta_i$ is the gradient of the constrained-area action integral. With neither θ_0 nor ν considered as degrees of freedom, the Hessian is tridiagonal. Fourth, ν is updated to satisfy $\nu = \langle\partial_2 S_i + \partial_1 S_{i+1}\rangle$, where $\langle\ldots\rangle$ denotes the average along the trial curve. The iterations are terminated when $\langle\partial_2 S_i + \partial_1 S_{i+1} - \nu\rangle$ is less than a small, user-supplied parameter.

The extremizing curves of the constrained-area action functional have been compared to periodic fieldlines of the pseudo field, with good agreement. It has been confirmed that both the radial location of the periodic fieldline on the $\theta = 0$ line and the numerical value of the action converge with second order accuracy in $h \equiv 1/N$, where N is the number of segments per 2π used in the piecewise-linear, piecewise-constant trial curves.

The algorithm for constructing the entire family of periodic pseudo fieldlines that comprise the rational pseudo surfaces proceeds as follows. It is particularly simple to find the symmetric, true, periodic fieldlines because we may constrain $\theta_0 = 0$ and $\nu = 0$. Furthermore, these fieldlines are identical to their reflections, i.e., $\theta(-\zeta) = -\theta(\zeta)$, and the periodicity condition, $\theta(2\pi q) = 2\pi p$, reduces to $\theta(\pi q) = \pi p$, which means that the pseudo fieldlines need only to be followed "half-way around."

The pseudo fieldline with $\theta_0 = \alpha$ serves as an initial guess for the pseudo fieldline with $\theta_0 = \alpha + d\alpha$, and we may trace out the entire pseudo surface by varying the poloidal angle constraint. Note that given that the (p, q) pseudo fieldlines have length equal to $2\pi q$, it is not required to construct the pseudo curves over the range $\alpha \in [0, 2\pi]$: periodicity means that it is only required to construct the curves over the range $\alpha \in [0, 2\pi/q]$.

B. Greene's residue

It is possible[22] to calculate Greene's residue[21] using the Lagrangian formulation. The residue is a measure of the stability of a given fieldline and is determined by the behavior of nearby fieldlines, $\theta_i + \delta\theta_i$, which are themselves determined by the *tangent dynamics*, defined by the derivatives of the equations of motion in Eq. (34)

$$\partial_{21} S_i\, \delta\theta_{i-1} + (\partial_{22} S_i + \partial_{11} S_{i+1})\, \delta\theta_i + \partial_{12} S_{i+1}\, \delta\theta_{i+1} = 0.$$

The multipliers, λ, are defined[22] by a tangent fieldline that grows exponentially, $\delta\theta_{i+q} = \lambda\,\delta\theta_i$, and thus satisfies $\sum_j M_{i,j}\,\delta\theta_j = 0$, where

$$M(\lambda) \equiv \begin{pmatrix} a_1 & b_1 & & & \lambda^{-1} b_q \\ b_1 & a_2 & b_2 & & \\ & . & . & . & \\ & & b_{q-2} & a_{q-1} & b_{q-1} \\ \lambda\, b_q & & & b_{q-1} & a_q \end{pmatrix}, \tag{37}$$

and $a_i \equiv \partial_{22} S_{i-1} + \partial_{11} S_i$ and $b_i \equiv \partial_{12} S_i$. The residue of a periodic fieldline is given by[22]

$$R = -\frac{1}{4}\, D\Pi^{-1}, \tag{38}$$

where $\Pi \equiv \prod_1^q (-b_i)$, and $D \equiv |M(1)|$ is the determinant of $M(1)$ and is given by

$$D = a_q |\Delta^1_{q-1}| - b_q^2 |\Delta^2_{q-1}| - b_{q-1}^2 |\Delta^1_{q-2}| - 2\Pi,$$

where $|\Delta^i_j|$ is the determinant of

$$\Delta^i_j \equiv \begin{pmatrix} a_i & b_i & & & \\ b_i & a_{i+1} & b_{i+1} & & \\ & . & . & . & b_{j-1} \\ & & & b_{j-1} & a_j \end{pmatrix}, \tag{39}$$

which is tridiagonal, and so $|\Delta^i_j|$ is easily computed using a recurrence relation

$$|\Delta^i_j| = a_j |\Delta^i_{j-1}| - b_{j-1}^2 |\Delta^i_{j-2}|. \tag{40}$$

It has been confirmed that the residue as computed by Eq. (38) converges with first order accuracy to that given by Eq. (13).

At this point, it is worth describing another algorithm for constructing the family of periodic pseudo fieldlines that comprise the rational pseudo surface. With the piecewise-linear representation for the periodic angle-curves, the area defined by Eq. (18) is

$$a = \left[\sum_{i=0}^{q-1} \theta_i + \pi p\right] \Delta\zeta - 2\pi p\, \pi q. \tag{41}$$

Rather than introducing a Lagrange multiplier to enforce the area constraint, the area constraint can be enforced directly by re-writing this equation in the form $\theta_{q-1} \equiv \theta_{q-1}(\theta_0, \ldots, \theta_{q-2}, a)$ and replacing θ_{q-1} as a independent degree of freedom by a. Then, the constrained-area action integral depends on $\boldsymbol{\theta} \equiv \{\theta_i : i = 0, q-2\}$ and a, i.e., $F \equiv F(\boldsymbol{\theta}; a)$. A curve is an extremum of the constrained-area action integral when $\mathbf{D}(\boldsymbol{\theta}; a) \equiv \nabla_{\boldsymbol{\theta}} F(\boldsymbol{\theta}; a) = 0$. The family of pseudo curves that comprises the pseudo surface may be constructed by varying a, which effectively shifts the extremal curve poloidally. For the curve to remain an extremum of $F \equiv F(\boldsymbol{\theta}; a)$ when a is varied, the curve must vary in order to satisfy $\mathbf{D}(\boldsymbol{\theta} + d\boldsymbol{\theta}; a + da) = 0$. This gives the poloidal integration equation

$$\frac{d\boldsymbol{\theta}}{da} = -(\nabla_{\boldsymbol{\theta}} \mathbf{D})^{-1} \cdot \partial_a \mathbf{D}. \tag{42}$$

Given one pseudo curve that lies on the pseudo surface, the entire family of pseudo curves can be traced out by integrating Eq. (42) around poloidally.

VI. APPLICATION TO LHD

We now consider a magnetic field of experimental interest. The LHD[12] is a 10-field period heliotron in operation at the National Institute for Fusion Science in Japan. LHD was designed to have nearly integrable magnetic fields, particularly near the magnetic axis; however, the magnetic field becomes chaotic near the plasma edge where low-order magnetic islands overlap. The magnetic fields consistent with finite-pressure, magnetohydrodynamic equilibria in LHD are routinely calculated using the HINT code[33] and its successor the HINT2 code.[34] In this work, for simplicity, we consider the magnetic field that is produced by current carrying coils external to the plasma domain as calculated by the Biot-Savart formula.

Shown in Fig. 1 is a Poincaré plot in cylindrical coordinates of the "standard" configuration. The rotational-transform varies from $\imath \approx 0.37$ on axis to $\imath \approx 2.00$ near the edge. Suitable initial toroidal coordinates are

$$R = 3.7 + 0.5\rho^{1/2}\cos(\theta) - 0.15\rho^{1/2}\cos(\theta - 10\,\zeta),$$
$$Z = -0.5\rho^{1/2}\sin(\theta) - 0.15\rho^{1/2}\sin(\theta - 10\,\zeta).$$

A. "Low resolution" chaotic coordinates

Using these initial toroidal coordinates, a selection of low-order QFM surfaces was constructed using the pseudo fieldline integration method. The selected periodicities are $(p, q) = (10, 25), (10, 24), (10, 23), \ldots (10, 7), (10, 6)$. These are shown as black lines in the lower half of Fig. 1.

By using these QFM surfaces as coordinate surfaces and introducing the straight pseudo fieldline angle, we can construct a new set of toroidal coordinates that can be thought of as straight-fieldline coordinates for an assumed, nearby, integrable field. The same Poincaré plot as in Fig. 1 is shown in the new coordinates in Fig. 2, except that only the region near the plasma edge between the (10, 7) and the (10, 5) islands is shown; the (10, 7) and (10, 6) islands are easy to identify, but the (10, 5) island chain is in a region of strong chaos and the (10, 5) separatrix is difficult to identify. An approximation to the separatrices of the (10, 7), the (20, 13) and the (10, 6) island chains as given by Eq. (23) is shown.

Recall that the construction of chaotic coordinates depends on the selection of rational QFM surfaces that form the coordinate framework; the coordinates formed by this selection of periodicities will be referred to as "low-resolution" chaotic coordinates. In this example, the QFM surfaces passing through the (10, 7) and (10, 6) *have* been used as part of the coordinate framework, and so these surfaces appear as flat lines in Fig. 2, as also would the (10, 8), (10, 9)…(10, 25) surfaces if the range of the figure was extended towards the magnetic axis; whereas the (20, 13)

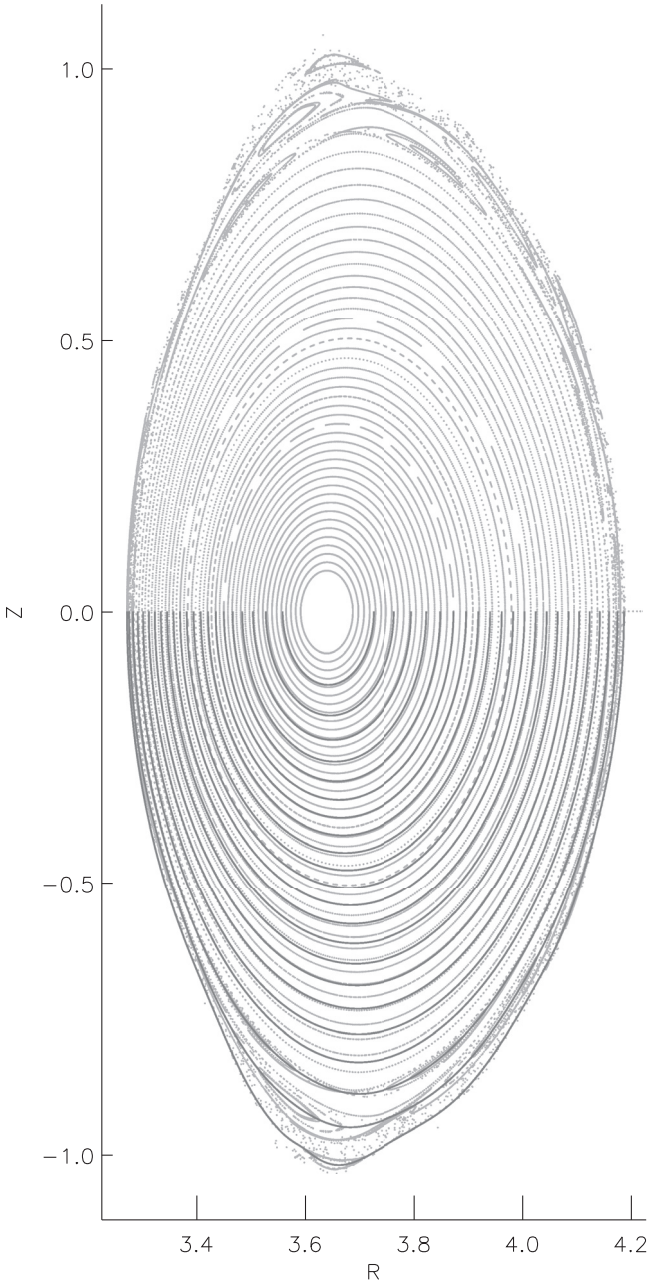

FIG. 1. Cylindrical coordinates: Poincaré plot (grey dots) of LHD showing a large volume of flux surfaces with some islands and chaos near the edge. The QFM surfaces chosen as the coordinate skeleton are shown (black lines).

QFM surface has *not*, and so the surface passing through the (20, 13) is not flat.

In these same, low-resolution coordinates, the constrained-area, action-extremizing method is used to construct various high-order periodic fieldlines that approximate either selected "intact" KAM surfaces or "broken," near-critical cantori. The selected periodicities are given by $(p, q) = (1230, 827), (1440, 953), (1440, 919), (1230, 772), (1230, 704), (1440, 809), (1310, 710), (1440, 775), (1230, 649)$, and $(850, 443)$, which approximate various noble irrationals. These periodic approximations to the irrational sets are shown as black dots in Fig. 2. The QFM surfaces that pass through these high-order rationals are not used as coordinate

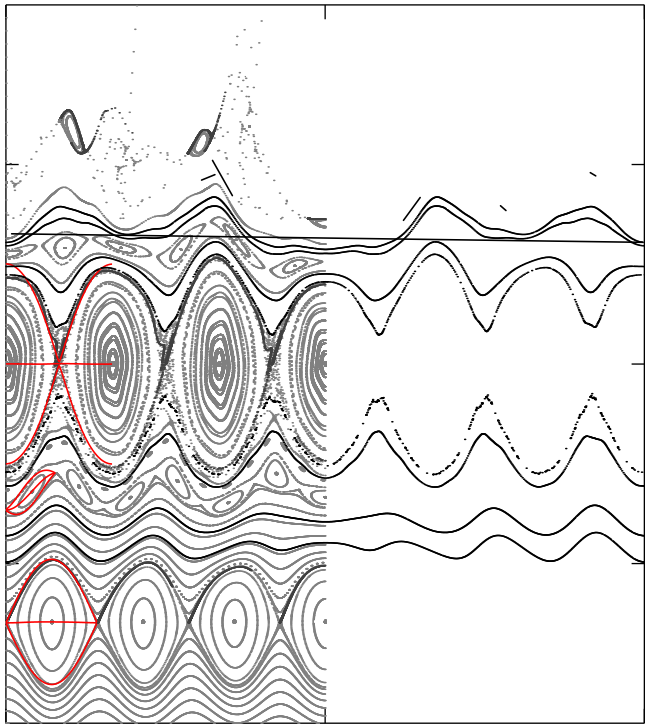

FIG. 2. Low-resolution chaotic coordinates: Poincaré plot (grey dots) showing the edge region of LHD. The (10, 7), (10, 13), and (10, 6) QFM surfaces are shown in red (only over one corresponding period of the island chain), as are the island separatrices. Approximations to the irrational flux surfaces and cantori are shown (black dots). The horizontal axis is the poloidal angle, $\theta \in [0, 2\pi]$, and the vertical axis is the radial coordinate $\equiv$ toroidal flux.

surfaces—an illustration of high-resolution chaotic coordinates is shown later—so these KAM surfaces and cantori do not coincide with coordinate surfaces and do not appear flat in Fig. 2.

A close examination of these high-order periodic orbits shows that some appear as closed curves in Fig. 2, as the finite number of dots are so close together, and some appear to have gaps. The former are good approximations to the KAM surfaces, which are perfect barriers, and the latter approximate the near-critical cantori, which are very strong, *partial* barriers.

This intuitive description can be made precise by an application of Greene's residue criterion. Here, we use the residue criterion to locate the outermost KAM surface, which we call the boundary surface. The algorithm[23,35] proceeds as follows. An inspection of the Poincaré plot, Fig. 2, suggests that the boundary surface is between the $(p_0, q_0) \equiv (10, 6)$ and the $(p_1, q_1) \equiv (10, 5)$ islands. Beginning from these "parent" rationals, a Farey Tree is constructed by recursively constructing the *mediant* $(p, q) \equiv (p_0 + p_1, q_0 + q_1)$, which divides the interval $[p_0/q_0, p_1/q_1]$ into two sub-intervals, $[p_0/q_0, p/q]$ and $[p/q, p_1/q_1]$. If $|R(p_0, q_0)| + |R(p, q)| < 0.5$, where $R(p, q)$ is the residue of the (p, q) periodic fieldline, then it is likely that at least one intact KAM surface with rotational-transform $\iota \in [p_0/q_0, p/q]$ exists. Because the locally most-robust KAM surfaces have *noble*-irrational rotational-transform, then if any irrational surfaces in this region exists then it is likely that the $\iota = (p_0 + \gamma p)/(q_0 + \gamma q)$ surface exists, where $\gamma = (1 + \sqrt{5})/2$ is the golden

mean. Similarly, if $|R(p,q)| + |R(p_1,q_1)| < 0.5$, then it is likely that the $\iota = (p_1 + \gamma p)/(q_1 + \gamma q)$ surface exists. By applying a recursive algorithm that examines the smaller and smaller intervals defined by successive mediants, this algorithm gives a very precise and definite approach for identifying the boundary surface. For this case, the boundary surface appears to be the $\iota \approx 1.895234$ surface, and the residues for the convergents of this irrational are shown in Fig. 3.

B. Anisotropic diffusion

To rigidly define the boundary surface as the "edge" of a magnetically confined plasma may be misguided in the study of confined plasmas. With *infinite* transport of temperature and pressure parallel to the magnetic field, it will be the case that the plasma boundary coincides with the boundary surface; however, for slightly non-ideal plasmas with small, but non-negligible, perpendicular transport, the near-critical cantori that will inevitably persist both inside and outside the boundary surface will provide barriers that may be as significant as that of the intact KAM surfaces.

To make these statements more concrete, consider the simple model of non-ideal transport described by the anisotropic diffusion equation, $\kappa_\parallel \nabla_\parallel T + \kappa_\perp \nabla_\perp T = 0$, where $\kappa_\parallel \gg \kappa_\perp$. Assuming coordinates for which the temperature is a surface function, $T \equiv T(\psi)$, the steady-state temperature gradient satisfies

$$T' \propto (\kappa_\parallel \varphi + \kappa_\perp G)^{-1}, \tag{43}$$

where φ is related to the quadratic flux and G is a geometric quantity.[36]

For all almost-invariant surfaces with $\varphi < \kappa_\perp G/\kappa_\parallel$, the temperature gradient is dominated by the perpendicular diffusion, just as what is the case for the temperature gradient across the invariant KAM surfaces. Not even the intact KAM surfaces are complete barriers when the transport is non-ideal; and there is hierarchy of partial barriers, both inside and outside the boundary surface, each of which corresponds to an almost-invariant surface. Furthermore, inside the boundary surface there will invariably be significant regions of poor confinement because of the presence of islands and chaotic fieldlines in non-ideal plasmas.

To quantify the hierarchy of partial barriers, we construct the "flux-Farey" tree,[2] shown in Fig. 4, beginning from the parent rationals $(p, q) = (10, 6)$ and $(10, 7)$. The

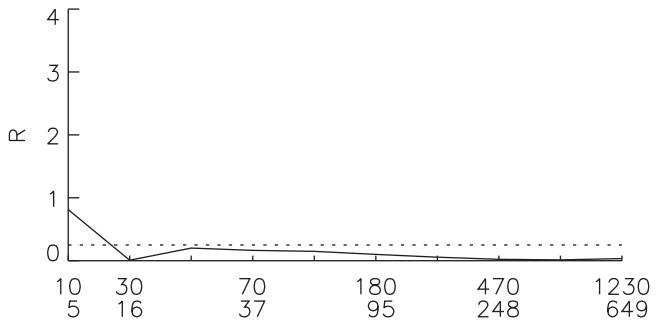

FIG. 3. Greene's residue for the rational convergents of the last closed flux surface.

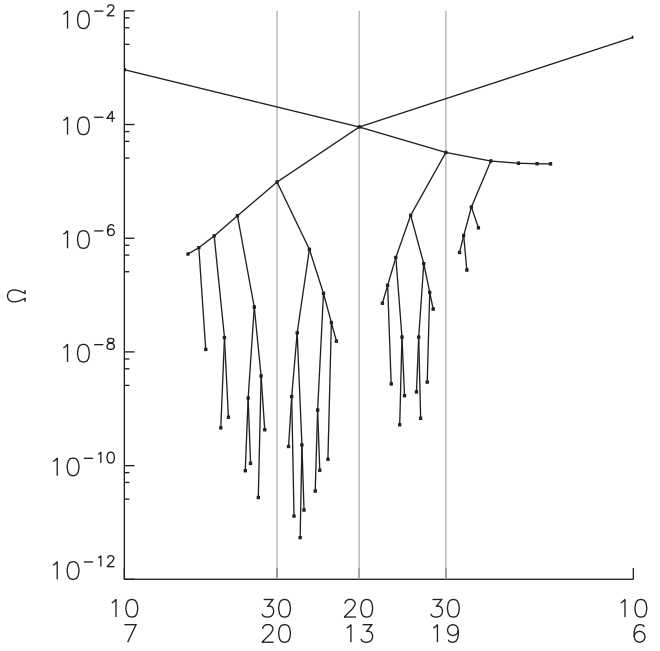

FIG. 4. The flux Farey tree formed by the (10, 7) and (10, 6) parent rationals: the outward-flux, $\Omega \equiv W_{p/q}$, across surfaces passing through the islands is shown against periodicity, (p, q).

flux, $\Omega \equiv W_{p/q}$ where $W_{p/q}$ is given by Eq. (24), across the (10, 6) and (10, 7) parent rationals is largest; and as one descends down the branches of this tree to the (20, 13), the (30, 19), (30, 20) rationals, etc., the flux across the rational surfaces typically decreases. If the flux approaches zero along some path down the Farey tree, then a KAM surface will exist; if not, the limiting value of Ω is the outward flux across the remnant cantorus, and the magnitude of Ω indicates the importance of that particular cantorus as a partial barrier. Noble irrationals are those particular irrationals that are obtained as limits of alternating paths down the Farey tree, and typically these have lower fieldline flux.

That the QFM surfaces can be chosen to arbitrarily closely approximate the KAM surfaces and the cantori[37] is of great practical importance because the KAM surfaces present *complete* barriers to radial fieldline transport, and the near-critical cantori are important *partial* barriers.[38] By choosing QFM surfaces with periodicities that approximate a selection of noble irrationals, the coordinate surfaces of chaotic coordinates can be chosen to coincide with isotherms of the anisotropic diffusion equation (this was demonstrated numerically[39] for the closely related[40,41] almost-invariant surfaces known as "ghost surfaces"[19,42–44]). With this being the case, the approximation $T \equiv T(\psi)$ leading to the derivation of Eq. (43) becomes more accurate.

C. "High resolution" chaotic coordinates

The idea of action-angle coordinates, and their extension to chaotic-coordinates, is to place all, or as much as is possible, of the geometric complexity of the dynamical system into the coordinates; so that in action-angle coordinates the dynamics appears simple, and in chaotic coordinates the dynamics appears as simple as possible.

Towards this aim, an additional set of higher-order surfaces is constructed as follows: (Step 1) Beginning with the low-resolution chaotic coordinates based on the $(p, q) = (10, 25), (10, 24), (10, 23), \ldots (10, 7)$ and $(10, 6)$ QFM surfaces, the QFM surfaces with periodicities given by the first 6 levels of the Farey trees beginning from the parent rationals (10, 8) and (10, 7), from the (10, 7) and (10, 6), and from the (10, 6) and (10, 5) parent rationals are constructed. These QFM surfaces are shown as black lines in Fig. 5. The Poincaré plot shown in Fig. 5 employs the low-resolution chaotic coordinates described earlier, and is essentially identical to Fig. 2 except that the vertical range has been extended slightly so that the (10, 8) island chain and separatrix (shown in red) can also be seen; recall that only the (10, 6), (10, 7), and (10, 8) QFM surfaces will appear flat in this figure, as the high-order QFM surfaces included in the first 6 levels of the Farey trees have not yet been used as coordinate surfaces.

(Step 2) Using these higher-order QFM surfaces as the foundation of a new coordinate framework, "high-resolution" chaotic coordinates can be constructed that are adapted more closely to the fractal structure of the magnetic field. The same Poincaré plot as shown in the low-resolution chaotic coordinates, namely, Figs. 2 and 5, is shown in the high-resolution chaotic coordinates in Fig. 6. In this figure, many high-order QFM surfaces are used in the coordinate framework and so more of the flux surfaces appear straight. Depending on how closely the selected QFM surfaces lie outside the separatrices of the low-order islands, the islands themselves become square.

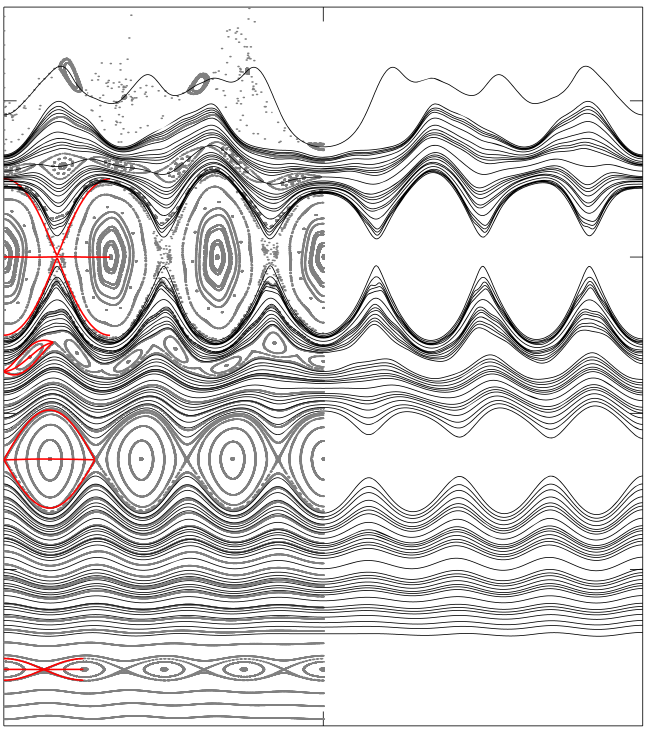

FIG. 5. Low-resolution chaotic coordinates: Poincaré plot (grey dots) of LHD showing the edge region. The (10, 8), (10, 7), (10, 13), and (10, 6) QFM surfaces are shown in red, as are the island separatrices. High-order QFM surfaces are shown (black lines). The horizontal axis is the poloidal angle, $\theta \in [0, 2\pi]$, and the vertical axis is the radial coordinate $\equiv$ toroidal flux.

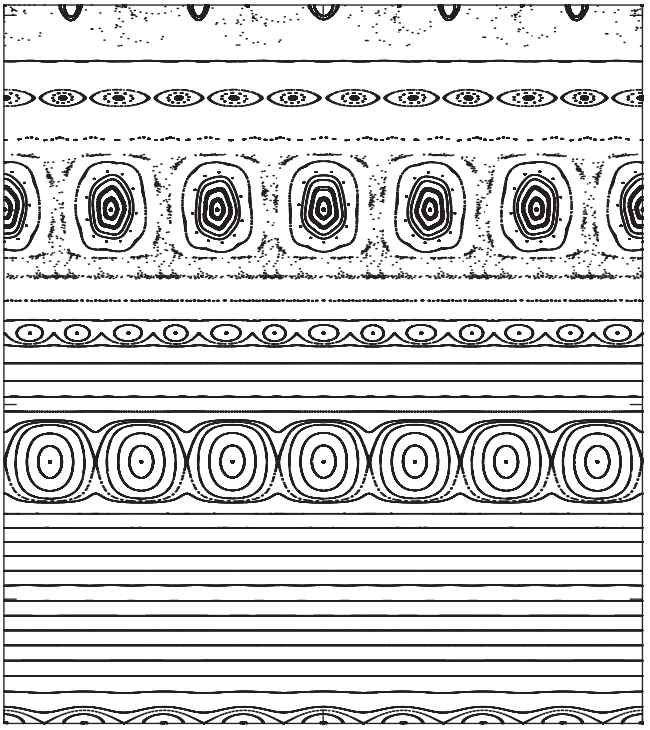

FIG. 6. High-resolution chaotic coordinates: Poincaré plot (grey dots) of LHD showing the edge region of LHD. The horizontal axis is the poloidal angle, $\theta \in [0, 2\pi]$, and the vertical axis is the radial coordinate $\equiv$ toroidal flux.

The vertical range of this figure extends from the (10, 8) QFM surface at the bottom to the (10, 5) QFM surface at the top. The upper half the (10, 8)-separatrix can be seen, as can the (10, 7), the (20, 13), the (10, 6), and the (20, 11) islands; but the separatrix of the (10, 5) island at the top of the figure cannot be clearly distinguished because this region of space is so strongly chaotic that the separatrix structure is not apparent. A close approximation to the boundary surface between the (20, 11) and the (10, 5) islands is also visible.

In these high-resolution coordinates, we may expect that the solutions to the anisotropic diffusion equation are approximated by a smoothed, fractal staircase described by Eq. (43); where the temperature gradients are locally maximum across the invariant and almost-invariant surfaces of locally minimal flux (i.e., the noble irrationals), and the gradients are reduced across the (rational) islands where φ is largest; and where the degree of smoothing is related to the non-ideal, perpendicular diffusion. As $\kappa_\perp \to 0$, the temperature gradient adopts a fractal structure, with singularities where the quadratic flux, φ, is zero.

VII. CONCLUDING COMMENTS

This paper has described chaotic coordinates as an extension of straight fieldline coordinates to non-integrable fields. These coordinates are based on a selection of almost-invariant, quadratic-flux minimizing surfaces that are labeled by their periodicity and that form a radial framework. In the limit as more rational surfaces are included, more of the

geometrical complexity of the dynamical system is absorbed into the coordinates and both the rational (i.e., the Poincaré-Birkhoff periodic orbits) and the irrational (i.e., the KAM surfaces and the cantori) fieldlines become straight, and it then follows that the islands become square. Such coordinates possibly have many applications, not only in the study of magnetically confined plasmas but also in other areas of physics that involve non-integrable Hamiltonian systems. Single-particle trajectories in a strong magnetic field can be described variationally,[45] and Lagrangian integration methods have been applied to guiding center calculations by Qin *et al.*[46,47]

The practical implementation of chaotic coordinates, and the determination of the boundary surface and the quantification of the strength of the hierarchy of partial barriers associated with the cantori, depends on efficiently and robustly constructing the periodic fieldlines and pseudo fieldlines that comprise the QFM surfaces. This paper has described a particularly fast construction of the pseudo fieldlines as constrained extrema of the magnetic fieldline action. This allows very high-order QFM surfaces to be constructed, so that as much of the geometrical complexity of the chaos can be absorbed into the coordinates as is possible; that is, until the geometrical complexity requires an exorbitant cost in numerical resolution and creates difficulties in the interpolation and extrapolation of the QFM surfaces that is required to construct smooth, global coordinates.

A. Robust interpolation and extrapolation

Regarding the numerics, there are two matters which should be considered in more detail: the interpolation between the QFM surfaces, and the extrapolation of the coordinates beyond the outermost QFM surface.

In the above, a Fourier description of each surface was constructed. This is itself is no problem as the surfaces are smooth; however, the interpolation between the coordinates is somewhat naive: the Fourier harmonics are interpolated by piecewise quintic polynomials; unfortunately, this does not guarantee that the interpolated surfaces do not intersect. Interpolating between extremely deformed surfaces, such as the high-order surfaces that lie just outside the separatrices of low-order islands, can be problematic. A better interpolation, perhaps, would be to use equipotential surfaces of the solution to Laplace's equation, $\nabla \cdot \nabla \Phi = 0$, with boundary condition $\Phi = 0$ and $\Phi = 1$ on the pair of adjacent QFM surfaces to be interpolated, as these surfaces are guaranteed to not intersect.

To extend the coordinates past the outermost constructed QFM surfaces, the present method extrapolates the Fourier harmonics. Given that all confinement devices are ultimately limited by a separatrix, and that the straight fieldline coordinates and their generalization to chaotic coordinates becomes singular, extrapolating into a singularity is unreliable. The nature of the singularity is understood: the singularity of the separatrix is like that of a pendulum, and so a more reliable extrapolation could exploit this in a fashion that is similar to how the "polar" singularity at the coordinate origin is treated (as described in the Appendix).

As a final comment, the discretization of the action integral in Sec. V allows for the numerical construction of ghost surfaces,[19] which are defined as an extension of ghost circles[42–44] to continuous time systems, and which are closely related to QFM surfaces.[19] Recently, a freedom in an angle transformation has been exploited to obtain a unification of these ostensibly different classes of almost-invariant surfaces.[40,48]

ACKNOWLEDGMENTS

This work was supported by DOE Grant No. DE-AC02-09CH11466. Dr. S. R. Hudson enjoyed the hospitality of the National Institute for Fusion Science during a three-month period in 2013, in which most of this work was performed.

APPENDIX: CONSTRUCTION OF VECTOR POTENTIAL

We begin with the magnetic field given in cylindrical coordinates

$$\mathbf{B} \equiv B^R \mathbf{e}_R + B^\phi \mathbf{e}_\phi + B^Z \mathbf{e}_Z, \tag{A1}$$

where B^R, B^ϕ, and B^Z are functions of (R, ϕ, Z). The coordinate basis vectors are $\mathbf{e}_R \equiv \partial \mathbf{x}/\partial R$, $\mathbf{e}_\phi \equiv \partial \mathbf{x}/\partial \phi$ and $\mathbf{e}_Z \equiv \partial \mathbf{x}/\partial Z$, where $\mathbf{x} \equiv R\cos\phi\,\mathbf{i} + R\sin\phi\,\mathbf{j} + Z\,\mathbf{k}$. An initial guess for magnetic coordinates, (ρ, θ, ζ), which are expressed via an inverse transformation

$$\begin{aligned} R &\equiv R(\rho, \theta, \zeta) \\ \phi &\equiv \zeta \\ Z &\equiv Z(\rho, \theta, \zeta). \end{aligned} \tag{A2}$$

Magnetic coordinates are necessarily "toroidal," by which it is meant that $\rho = 0$ coincides with the magnetic axis, and θ and ζ are angles that, respectively, increase by 2π along curves that loop the short way and the long way around the torus. Toroidal coordinates provide some computational advantages, but also present difficulties because of the coordinate singularity at $\rho = 0$. To illustrate the nature of the singularity, it is convenient to define "Cartesian-like" and "polar-like" coordinates via $x \equiv r\cos\theta \equiv R(\rho, \theta, \zeta) - R_0(\zeta)$ and $y \equiv r\sin\theta \equiv Z(\rho, \theta, \zeta) - Z_0(\zeta)$, where (R_0, Z_0) is the magnetic axis, and to assume that an arbitrary, magnetic vector potential may be written

$$\mathbf{A} = A_x \nabla x + A_y \nabla y + A_\zeta \nabla \zeta + \nabla g, \tag{A3}$$

where $A_x(x, y, \zeta)$, $A_y(x, y, \zeta)$, $A_z(x, y, \zeta)$, and the as-yet-arbitrary gauge function, $g(x, y, \zeta)$, are regular at $x = y = 0$, e.g., $A_x = \sum_{i,j} \alpha_{i,j}(\zeta)\, x^i y^j$, for small x and small y.

The expressions for A_x, A_y, A_ζ, and g can be cast as functions of (r, θ, ζ) by repeated applications of the double-angle formula to obtain

$$\begin{aligned} A_x &= \sum\nolimits_m r^m a_m(s)\sin(m\theta), \\ A_y &= \sum\nolimits_m r^m b_m(s)\cos(m\theta), \\ A_\zeta &= \sum\nolimits_m r^m c_m(s)\cos(m\theta), \\ g &= \sum\nolimits_m r^m g_m(s)\cos(m\theta), \end{aligned} \tag{A4}$$

where $a_m(s)$, $b_m(s)$, $c_m(s)$, and $g_m(s)$ are power series in $s \equiv r^2$, e.g., $a_m(s) \equiv \sum_i a_{m,i} s^i$, $b_m(s) \equiv \sum_i b_{m,i} s^i$, $c_m(s) \equiv \sum_i c_{m,i} s^i$, and $g_m(s) \equiv \sum_i g_{m,i} s^i$; and we have restricted attention to stellarator-symmetric geometry and the dependence on ζ is suppressed. A similar analysis is valid for the coordinate functions defined in Eq. (A2), and regularity factors r^m are included in both the coordinate transformation and in the vector potential harmonics.

The Cartesian-to-polar transformation, $x = r\cos\theta$ and $y = r\sin\theta$, induces the vector transformation $\nabla x = \cos\theta\nabla r - r\sin\theta\nabla\theta$ and $\nabla y = \sin\theta\nabla r + r\cos\theta\nabla\theta$, and

$$\mathbf{A} = A_r\nabla r + A_\theta\nabla\theta + A_\zeta\nabla\zeta + \partial_r g\nabla r + \partial_\theta g\nabla\theta + \partial_\zeta g\nabla\zeta. \tag{A5}$$

To lowest order in r, the radial component is

$$A_r = r^0(b_{0,0} + g_{1,0})\sin\theta + r^1(a_{1,0}/2 + b_{1,0}/2 + 2g_{2,0})\sin 2\theta + r^2(a_{2,0}/2 + b_{2,0}/2 + 3g_{3,0})\sin 3\theta + \cdots,$$

which is eliminated by the gauge choice

$$\begin{aligned} g_{1,0} &= -b_{0,0}, \\ g_{2,0} &= -(a_{1,0}/2 + b_{1,0}/2)/2, \\ g_{3,0} &= -(a_{2,0}/2 + b_{2,0}/2)/3. \end{aligned} \tag{A6}$$

Order-by-order, A_r can be eliminated using the freedom in the $g_{m,i}$ to obtain

$$\mathbf{A} = A_\theta\nabla\theta + A_\zeta\nabla\zeta. \tag{A7}$$

The expressions for A_r and A_θ are coupled, and the choice of gauge in Eq. (A6) entails

$$A_\theta = \sum\nolimits_m r^{m+2} f_m(s)\cos(m\theta), \tag{A8}$$

where the $f_m(s)$ are arbitrary polynomials in s. The $g_{m,i}$ for $m = 0$ are not constrained by Eq. (A6); this remaining, "toroidal" gauge-freedom can be used to simplify A_ζ, so that $c_{m,i} = 0$ for $m = 0$.

With the vector potential given by Eq. (A7), the equation $\mathbf{B} = \nabla\times\mathbf{A}$ reduces to

$$\sqrt{g}B^\rho = \partial_\theta A_\zeta - \partial_\zeta A_\theta, \quad \sqrt{g}B^\theta = -\partial_\rho A_\zeta, \quad \sqrt{g}B^\zeta = \partial_\rho A_\theta. \tag{A9}$$

Given B^θ and B^ζ, the components of the vector potential can be determined by radially integrating outwards from the coordinate axis, $A_{\theta,j} = \int^\rho (\sqrt{g}B^\zeta)_j\, d\rho$ and $A_{\zeta,j} = -\int^\rho (\sqrt{g}B^\theta)_j\, d\rho$, where j labels each Fourier harmonic. The third equation in Eq. (A9) is satisfied if $\partial_\rho(\sqrt{g}B^\rho) + \partial_\theta(\sqrt{g}B^\theta) + \partial_\zeta(\sqrt{g}B^\zeta) = 0$, i.e., if $\nabla\cdot\mathbf{B} = 0$. Note that it is usually quite easy to locate the magnetic axis given the field in cylindrical coordinates by finding the magnetic fieldline that closes upon itself after one toroidal period; however, this might become complicated if two magnetic axes are present, such as what might be the case in applications modeling sawteeth, for example.

A simple approach for constructing a convenient numerical representation is to construct A_θ and A_ζ on a regular radial grid by radial integration, i.e., to obtain $A_\theta(\rho_i,\theta,\zeta) \equiv \sum_j A_{\theta,j,i}\cos(m\theta - n\zeta)$ and similarly for A_ζ, where $\rho_i \equiv i\Delta\rho$. Then, the Fourier components, $A_{\theta,j,i}$ and $A_{\zeta,j,i}$ can be radially interpolated, by a piecewise-cubic interpolation for example, where the derivatives are determined using finite-differences, e.g., $\partial_\rho A_{\theta,j,i} \equiv (A_{\theta,j,i+1} - A_{\theta,j,i-1})/2\Delta\rho$.

However, given that what really is required is that the appropriate derivatives of the vector potential match the magnetic field as closely as possible at finite numerical resolution, a more accurate interpolation and more efficient radial-integration construction is possible. Consider the interpolation $f(\rho) = \sum_k f^k \varphi_k(\bar\rho)$, where the f^k are fitting parameters and the $\varphi_k(\bar\rho)$ are the piecewise *quintic* polynomials, and the local domain of the interpolation is $\bar\rho \equiv (\rho - \rho_i)/\Delta\rho$ for $\rho \in [\rho_{i-1}, \rho_i]$. We require $f'(\rho) = y(\rho)$, where $f \equiv A_{\theta,j}$ and $y \equiv (\sqrt{g}B^\zeta)_j$, and similarly for $A_{\zeta,j}$ and $\sqrt{g}B^\theta$. By choosing a set of points, ρ, in $[\rho_{i-1}, \rho_i]$, the fitting parameters are determined by a matrix equation $\sum_k f^k \varphi_k'(\rho) = y(\rho)$. This ensures that the radial derivative equations in Eq. (A9) are satisfied *exactly* on the ρ. We have chosen a piecewise quintic interpolation for the Fourier harmonics of $\mathbf{A}$ because both the pseudo fieldline integration and the constrained-area action minimizing methods for locating periodic pseudo-fieldlines exploit the derivatives of the field, and is it preferable to have a smooth representation for $\mathbf{B}$.

[1] H. Goldstein, *Classical Mechanics*, 2nd ed. (Addison-Wesley, Massachusetts, 1980).
[2] J. D. Meiss, Rev. Mod. Phys. **64**, 795 (1992).
[3] D. K. Arrowsmith and C. M. Place, *An introduction to Dynamical Systems* (Cambridge University Press, Cambridge, UK, 1991).
[4] A. J. Lichtenberg and M. A. Lieberman, *Regular and Chaotic Dynamics*, 2nd ed. (Springer-Verlag, New York, 1992).
[5] S. Aubry, Physica D **7**, 240 (1983).
[6] J. N. Mather, Topology **21**, 457 (1982).
[7] A. N. Kolmogorov, Dokl. Akad. Nauk. SSR **98**, 469 (1954).
[8] V. I. Arnold, Russ. Math. Surv. **18**, 9 (1963).
[9] J. Moser, Nachr. Akad. Wiss. Göttingen, Math. Phys. Kl. II **1962**, 1.
[10] K. Tomabechi, J. R. Gilleland, Y. A. Sokolov, R. Toschi, and the ITER Team, Nucl. Fusion **31**, 1135 (1991).
[11] C. Beidler, G. Grieger, F. Herrnegger, E. Harmeyer, J. Kisslinger, W. Lotz, H. Maassberg, P. Merkel, J. Nuhrenberg, F. Rau *et al.*, Fusion Technol. **17**, 148 (1990).
[12] A. Iiyoshi, M. Fujiwara, O. Motojima, N. Ohyabu, and K. Yamazaki, Fusion Technol. **17**, 169 (1990).
[13] J. D. Hanson and J. R. Cary, Phys. Fluids **27**, 767 (1984).
[14] S. R. Hudson and R. L. Dewar, Phys. Lett. A **226**, 85 (1997).
[15] T. E. Evans, R. A. Moyer, P. R. Thomas, J. G. Watkins, T. H. Osborne, J. A. Boedo, E. J. Doyle, M. E. Fenstermacher, K. H. Finken, R. J. Groebner *et al.*, Phys. Rev. Lett. **92**, 235003 (2004).
[16] R. L. Dewar, S. R. Hudson, and P. Price, Phys. Lett. A **194**, 49 (1994).
[17] S. R. Hudson, D. A. Monticello, A. H. Reiman, A. H. Boozer, D. J. Strickler, S. P. Hirshman, and M. C. Zarnstorff, Phys. Rev. Lett. **89**, 275003 (2002).
[18] M. C. Zarnstorff, L. A. Berry, A. Brooks, E. Fredrickson, G. Y. Fu, S. Hirshman, S. Hudson, L.-P. Ku, E. Lazarus, D. Mikkelsen *et al.*, Plasma Phys. Controlled Fusion **43**, A237 (2001).
[19] S. R. Hudson and R. L. Dewar, J. Plasma Phys. **56**, 361 (1996).
[20] J. N. Mather, Publ. Math. I.H.E.S. **63**, 153 (1986).
[21] J. M. Greene, J. Math. Phys. **20**, 1183 (1979).
[22] R. S. MacKay and J. D. Meiss, Phys. Lett. A **98**, 92 (1983).
[23] J. M. Greene, R. S. MacKay, and J. Stark, Physica D **21**, 267 (1986).
[24] J. R. Cary and R. G. Littlejohn, Ann. Phys. **151**, 1 (1983).
[25] R. S. MacKay, Nonlinearity **5**, 161 (1992).
[26] I. Niven, *Irrational Numbers* (The Mathematical Association of America, USA, 1956).

[27]B. Chirikov, Phys. Rep. **52**, 263 (1979).
[28]W. D. D'haeseleer, W. N. G. Hitchon, J. D. Callen, and J. L. Shohet, *Flux Coordinates and Magnetic Field Structure* (Springer, Berlin, 1991).
[29]A. H. Boozer, Phys. Fluids **25**, 520 (1982).
[30]J. R. Cary and J. D. Hanson, Phys. Fluids B **3**, 1006 (1991).
[31]S. R. Hudson, Phys. Rev. E **74**, 056203 (2006).
[32]R. L. Dewar and S. R. Hudson, Physica D **112**, 275 (1998).
[33]K. Harafuji, T. Hayashi, and T. Sato, J. Comput. Phys. **81**, 169 (1989).
[34]Y. Suzuki, N. Nakajima, K. Watanabe, Y. Nakamura, and T. Hayashi, Nucl. Fusion **46**, L19 (2006).
[35]R. S. MacKay and J. Stark, Nonlinearity **5**, 867 (1992).
[36]S. R. Hudson, Phys. Plasmas **16**, 010701 (2009).
[37]I. C. Percival, "Variational principles for invariant Tori and Cantori," *AIP Conference Proceedings No. 57*, edited by M. Month and J. C. Herra (AIP, New York, 1979).
[38]R. S. MacKay, J. D. Meiss, and I. C. Percival, Phys. Rev. Lett. **52**, 697 (1984).
[39]S. R. Hudson and J. Breslau, Phys. Rev. Lett. **100**, 095001 (2008).
[40]R. L. Dewar, S. R. Hudson, and A. M. Gibson, Plasma Phys. Controlled Fusion **55**, 014004 (2013).
[41]S. R. Hudson and R. L. Dewar, Phys. Lett. A **373**, 4409 (2009).
[42]C. Golé, J. Differ. Equations **97**, 140 (1992).
[43]R. S. MacKay and M. R. Muldoon, Phys. Lett. A **178**, 245 (1993).
[44]C. Golé, *Symplectic Twist Maps: Global Variational Techniques* (World Scientific, 2001).
[45]R. G. Littlejohn, J. Plasma Phys. **29**, 111 (1983).
[46]H. Qin and X. Y. Guan, Phys. Rev. Lett. **100**, 035006 (2008).
[47]H. Qin, X. Guan, and W. M. Tang, Phys. Plasmas **16**, 042510 (2009).
[48]R. L. Dewar, S. R. Hudson, and A. M. Gibson, Commun. Nonlinear Sci. Numer. Simul. **17**, 2062 (2012).